18th Australasian Fluid Mechanics Conference
Launceston, Australia
3-7 December 2012

Secondary flow in stratified open channel flow on a bend

N. Williamson[1], **S. E. Norris**[2], **S. W. Armfield**[1] **and M. P. Kirkpatrick**[1]

[1]School of Aerospace, Mechanical and Mechatronic Engineering,
The University of Sydney, New South Wales 2006, Australia

[2]Department of Mechanical Engineering
University of Auckland, Auckland 1142, New Zealand

Abstract

This work examines the effect of stratification on open channel flow around bends. We use direct numerical simulation of fully turbulent, two–layer stratified flow, in an idealised open channel with rectangular cross-section and a 120 degree bend, with a radius to channel breadth ratio of 1.5. The bulk Richardson number for the flow is 2.4. We additionally perform a non-stratified DNS simulation of the same flow.

Our stratified flow results compare well with published field studies in estuaries. The near bed measurements provided by our DNS simulations demonstrate a quite novel observation, that even in stratified conditions, the shear stress in the channel base is inwards directed, the same as for the non-stratified flows. Previous field studies of estuaries have not obtained such near bed measurements. This has important implications for near bed transport of sediment and cross stream circulation.

We show that stratification can introduce strong variation in vertical shear magnitude and orientation across the mixing layer. At the bottom and at the top of the mixing layer, the vertical shear is directed towards the outer side wall. In the center of the mixing layer it is oriented towards the inner wall.

Introduction

In rivers and estuaries, the flow on bends produces important mixing and sediment entrainment behaviour that is critical to overall understanding of the river or estuary system [1]. Stable density stratification, which could be produced by either surface heating or saline ocean or groundwater intrusions, can significantly modify these behaviours [2, 3, 4, 5]. At present many aspects of these flows are not well understood and limit the applicability of flow modelling parameters such as entrainment rate or eddy viscosity.

On a channel bend, the secondary flow generated by a depth varying centrifugal force, is relatively well understood in non-stratified flow. Field studies in estuaries have shown that the flow behaviour in stratified conditions can be far more complex [2, 4, 5]. The secondary flow acts to raise the lower dense fluid towards the inside of the bend. The tilted density interface is then subjected to a baroclinic restoring (outwards directed) force, which is also depth varying. In a recent estuarine field study, it was shown that the interaction of the secondary circulation and the restoring baroclinic force produces a complex three-layer circulation pattern under conditions of strong stratification [5]. The stream-wise variation in the relative strength of these forces results in a downstream adjustment of the flow which is not well understood [2, 3, 4, 5].

Recent small scale numerical simulations of isothermal open channel flows have been successfully used as canonical models of river systems [6, 7]. In the present study we use direct numerical simulations of small scale open channel flow on a bend, with and without an imposed density stratification, to examine how cross-stream circulation develops around a channel bend. We examine flow where the bend is sharp and the stratification has a sharp two-layer density profile. In Australian river systems, such a flow might be expected where saline water is purged from a hyper-saline deep river pool into the main channel [8, 9, 10]. The mixing behaviour of these intrusions and their persistence downstream are of interest to environmental managers of these river systems.

Governing Equations

Results for two direct numerical simulations of open channel flow on a bend are presented in this study. The first is a density stratified flow and the second is an isothermal flow in which there is no scalar transport. The geometry of the simulation domain is an open rectangular channel with a short initial straight section of length $L/D = 1$, followed by a 120° bend and then a second straight section of length $L/D = 2$. The channel width is $W/D = 3$ and the bend radius to width ratio is $R/W = 1.5$ where the radius is taken from the center of the channel ($W/2$).

In these simulations we solve the three dimensional Navier–Stokes equations for an incompressible fluid with the Oberbeck-Boussinesq approximation for buoyancy. These equations for the conservation of mass, momentum and temperature ϕ can be written as

$$\nabla \cdot \mathbf{u} = 0, \tag{1}$$

$$\frac{\partial \mathbf{u}}{\partial t} + \nabla \cdot (\mathbf{uu}) = -\nabla p + \frac{1}{Re}\nabla^2 \mathbf{u} - Ri_b \phi, \tag{2}$$

and

$$\frac{\partial \phi}{\partial t} + \nabla \cdot (\mathbf{u}\phi) = \frac{1}{RePr}\nabla^2 \phi, \tag{3}$$

respectively. The governing non-dimensional parameters are the bulk Reynolds number $Re = U_b D/\nu = 7500$ and for the stratified flow, the Prandtl number $Pr = \nu/\alpha = 1.5$, bulk Richardson number $Ri_b = \sigma D/U_b^2 = 2.4$ where $\sigma = \Delta\Phi_0 \beta g$ is the reduced gravity. The gravitational acceleration vector (aligned with the negative y direction) is given by g and β is the coefficient of thermal expansion. ν and α are the kinematic viscosity and scalar diffusivity of the fluid. The equations are made non-dimensional by the bulk channel velocity U_b, the channel depth D and the temperature difference at the inlet $\Delta\Phi_0 = \Phi_H - \Phi_C$, where Φ_C and Φ_H are the temperatures of the lower cold layer and upper hot layer respectively. The resulting non-dimensional velocity, length, time, pressure and temperature are denoted by lower–case and given as $u = U/U_b$, $x = X/D$, $t = TU_b/D$, $p = P/\rho U_b^2$ and $\phi = (\Phi - \Phi_H)/(\Phi_C - \Phi_H)$. Dimensional values are upper–case.

The equations are solved using *ALE*, an unstructured finite volume solver described in detail by [11]. The code uses a cell-centred co-located storage arrangement for flow variables, with cell-face velocities calculated using the Rhie-Chow momentum interpolation. We use a structured orthogonal mesh. The spatial derivatives are discretised using second order central finite differences except for the scalar advective term which uses second order central finite differences with the ULTRA flux limiter. The Adams-Bashforth time advancement scheme is used for the non-linear terms and Crank-Nicolson for the time advancement of the diffusive terms. The pressure correction equation is solved using a stabilised Bi-conjugate gradient solver with an incomplete Cholesky factorisation preconditioner [12]. The momentum and temperature equations are solved using a Jacobi solver.

At the inlet to the domain, the upstream stream-wise (s) boundary, a time-varying velocity field is re-played as the inlet boundary condition. This field is obtained from a previous DNS simulation of periodic open straight channel flow with the same bulk Reynolds number. The flow entering the domain is then fully developed, unsteady turbulent isothermal open channel flow. At the inlet the temperature field is set as a step function given in equation 4.

$$\phi = \begin{cases} 1 & \text{for } 0 < y < 0.17 \\ 1-(y-0.17)/0.06 & \text{for } 0.17 \leq y < 0.23 \\ 0 & \text{for } 0.23 \leq y \end{cases} \quad (4)$$

The downstream stream-wise boundary is 'open' where stream-wise gradients in all velocity components and temperature are set to zero. In the span-wise (r) direction the domain is bounded by no-slip side walls. The bottom boundary ($y = 0$) is also a no-slip wall. The top boundary ($y = 1$) approximates a free surface with a slip wall condition, i.e. $\partial u_s/\partial y = 0$, $\partial u_r/\partial y = 0$ and $u_y = 0$.

In stream–wise (s), wall–normal (y) and span–wise (r) directions, the grid has $[n_s, n_y, n_r] = [456, 85, 180]$ nodes with $\Delta y = 0.00025 - 0.015$ and $\Delta r = 0.00025 - 0.021$. In the stream-wise direction $\Delta s = 0.025$ at $r = 4.5$ from the inlet to the start of the bend. On the bend $\Delta s = r\Delta\theta$, where θ is the angular location on the bend, so the grid is linearly stretched between $\Delta s = 0.0166 - 0.0333$ over $r = 3 - 6$ with the transform to a cylindrical coordinate system. Following the bend, in the second straight section, the grid is expanded in the stream-wise direction with a constant 5% growth rate. This second straight region provides a buffer between the outlet and the bend. The flow in this region is not examined in this study.

In most rivers and estuaries the scalar diffusivity is low resulting in $Pr \sim 7$ for thermal diffusivity in water and $Pr \sim 700$ for salinity diffusivity. In this study we have arbitrarily taken $Pr = 1.5$ to limit the resolution requirements of the simulations as the Batchelor scale $\eta_p = \eta/\sqrt{Pr}$, where η is the Kolmogorov length scale. A time step of $\Delta t = 0.00025$ was used with the Courant number ranging between $0.03 - 0.06$. The simulations were performed until the flow was fully developed and then simulations were advanced for a further non-dimensional simulation time of $t = 70$, approximately 6 complete turnovers of fluid in the domain.

Results

In examining the flow results in the bend we adopt a cylindrical coordinate system with angular location θ, radial location r and vertical location y. The velocity components are therefore u_θ, u_y, u_r. Time averaged quantities are denoted by an over-bar.

In figure 1, contours of the time averaged stream-wise vorticity defined as, $\omega_\theta = \partial\overline{u}_y/\partial r - \partial\overline{u}_r/\partial y$ are shown at $\theta = 45^\circ$. In figure 1 *(a)* the isothermal flow result is presented. The center of the channel is dominated by a circulation cell generated by the depth varying centrifugal force. Near the outer wall at the surface is a smaller circulation cell, termed an 'outer bank cell' [1]. In figure 1 *(b)*, the stratified flow is shown, with a contour line of $\overline{\phi} = 0.5$ given as an indication of intrusion height. Above the intrusion the flow is qualitatively similar to the isothermal flow, with the same circulation cell in the channel center and the smaller outer bank cell. Immediately below the thermocline or density interface, the radial component of the flow is outward directed while near the channel bottom at the wall the flow is again inward directed.

There are similarities between this stratified flow result and the estuarine field result reported in [5] under conditions of strong stratification. In that study the authors reported what they termed a three layer flow where the radial component of flow near the surface is oriented in the same direction as that below the pycnocline. The implication of that result is that the near bed velocity is also outwards oriented. The present study finds a similar result, however near the base of the channel we observe an additional very thin layer of inwards directed flow, forming a fourth layer, completing an additional circulation cell. The field measurements in [5] do not extend below $y = 0.05$, the region over which this layer is observed. The favourable comparison of our numerical simulations and the field study over the region where both measurements coincide suggests that the near bed behaviour we observe in our study may also be present in these estuary flows. This has important implications for sediment transport and entrainment behaviour. It implies that in stratified flow, the mean near bed erosion forces act towards the inner side wall, the same as in non-stratified flow, but with reduced strength. The ultimate sediment transport balance across the channel is a more complex issue as the radial flow just below the interface is outward directed but this is beyond the scope of this study.

To underline this result we plot contours of the mean wall shear stress τ_w in figure 2, where both radial and stream-wise components are included. The shear stress is oriented to the inside of the channel for both isothermal and thermal flows, indicating that the radial component of the velocity is inwards directed though out the channel bend. The scaled vectors and contours indicate that the lateral component is much more significant in the isothermal case however. The total combined shear is also reduced with τ_w peaking at 0.0106 for the isothermal flow compared with an almost constant result of $\tau_w \approx 0.0036$ around the bend for the stratified flow. The Reynolds number based on wall shear stress or friction velocity is $Re_\tau = 400 - 500$ for the stratified flow.

We examine the stream-wise development of the lateral circulation around the bend with reference to figure 3, where the mean velocity field at the center of the channel ($r = 4.5$) is plotted with streamwise location between $\theta = 5 - 115^\circ$. For the stratified flow we also refer to figure 4, where we plot the local gradient Richardson number, Ri_g, with height at five locations between $\theta = 5 - 115^\circ$ at $r = 4.5$. Ri_g is defined here as,

$$Ri_g = \frac{-Ri_b(\partial\overline{\phi}/\partial y)}{(\partial\overline{u}_\theta/\partial y)^2 + (\partial\overline{u}_r/\partial y)^2}. \quad (5)$$

On the same figure $\overline{\phi}$ is plotted together with γ, the orientation of mean vertical shear in the flow, with respect to the stream-wise direction

$$\gamma = \arctan\left(\frac{\partial\overline{u}_r/\partial y}{\partial\overline{u}_\theta/\partial y}\right). \quad (6)$$

In both the isothermal flow and stratified flows, at the entrance to the bend at $\theta = 5$, the stream-wise and radial velocity profiles are similar as the flow begins to adjust to the centrifugal forcing (figure 3). Over $\theta = 5 - 30$, the flow behaviours differ. In

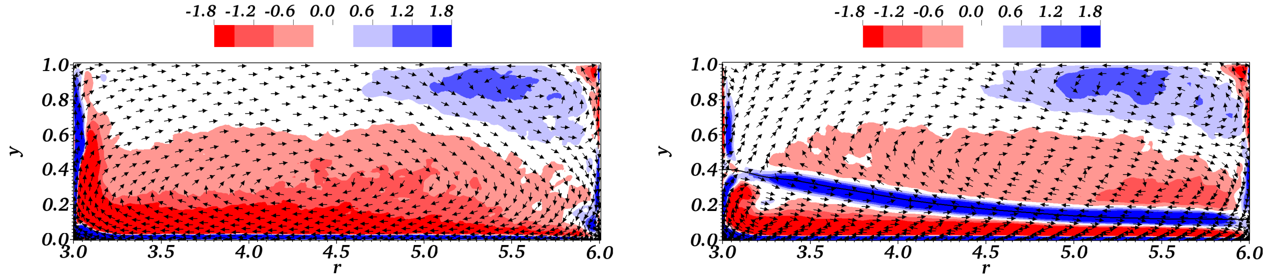

(a) (b)

Figure 1: Contours of mean stream-wise vorticity, ω_θ, at $\theta = 45^\circ$ for the isothermal flow result *(a)* and stratified flow *(b)*. Scale is given in the figures. Overlaid velocity vectors are not to scale.

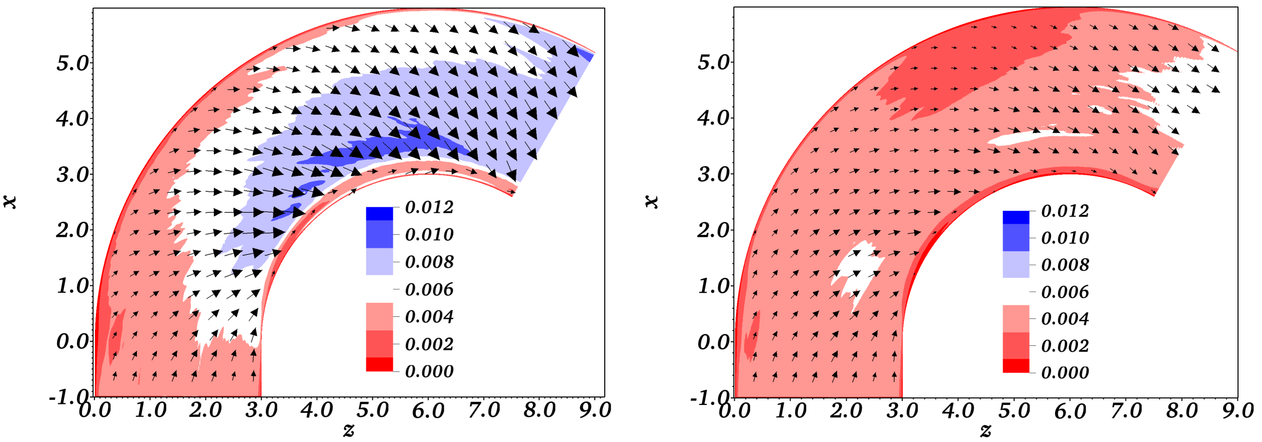

(a) (b)

Figure 2: Contours of mean wall shear, τ_w, for the isothermal flow result *(a)* and stratified flow *(b)*. Scale is given in the figures. Overlaid shear vectors are to scale.

the isothermal flow the helical flow structure continues to develop over the center of the channel. In the stratified flow the density interface is raised towards the inner channel side wall and the baroclinic restoring force acts against the centrifugal forcing. The four layer structure is apparent with the radial velocity oriented towards the outer wall just below the interface and at the top of the channel, and oriented towards the inner wall at the channel base and just above the density interface. Over $\theta = 30-120^\circ$ these circulation cells are maintained. The radial velocity in the near bed region of the isothermal flow is much greater than the stratified flow. The stream-wise velocity profiles in both flows are very flat in the region above the interface. In the stratified flow the stream-wise velocity decreases markedly compared with the isothermal flow.

In the stratified flow over $\theta \approx 0-25^\circ$, $\gamma \approx 0$ over most of the thermocline so the radial shear is low (figure 4). The interface is sharp and Ri_g is large, so the stratification is very stable. Over $\theta = 25-120^\circ$, as the lateral circulation cells develop, the four layer structure of the flow introduces a complex forcing on the mixing layer. The radial velocity profile $\overline{u}_r$ varies strongly through the thermocline as shown in figure 3. Just above and below the mixing layer the radial component of shear is oriented towards the outer side wall. Through the center of the interface, near the location where $\phi = 0.5$, the orientation is towards the inner side wall. At the bottom of the mixing layer $\gamma \approx +65$, while at the center of the mixing layer where $\phi \approx 0.5$ $\gamma \approx -72$ and at the bottom of the mixing layer the orientation returns to $\gamma \approx +65$, resulting in a total change in orientation of about 200 degrees.

Ri_g rises to peaks at the two locations where γ passes through 0° and shear is due only to the stream-wise component. These peaks appear to coincide with the extremities of the mixing layer. Between the locally high values of Ri_g is a local minimum point of Ri_g which also approximately coincides with the location where $\phi = 0.5$ and where the shear is orientated towards the inner side wall and $\gamma < 0$.

At the center of the mixing layer $Ri_g > 1$ until $\theta \approx 57^\circ$. At $\theta = 30^\circ$, the mixing activity is not observed to be intense in any part of the intrusion, with $Ri_g \approx 10$ in the center of the interface. We can report that large eddies in the over-flow can be seen impinging on the interface which advect the diffuse fluid from the upper part of the mixing layer into the overflow. By $\theta = 60^\circ$, the interface is more active with the mean gradient Richardson number at the interface $Ri_g \approx 0.8$. At this location, intermittent oscillations move through the interface some of which have K-H or Holmboe appearance. At $\theta = 90^\circ$, with the same mean gradient Richardson number as at $\theta = 60^\circ$, the interface is more energetic with K-H like waves observed in the center of the interface. These oscillations appear with circulation with $\omega_\theta > 0$, with shear towards the inner side wall. At the top of the thermocline, similar K-H structures are observed with the opposite rotation. Similar behaviour is observed intermittently in the lower region. In both these locations the vorticity of the oscillations or waves is consistent with the mean shear observed in these locations. In this way mean shear and Ri_g profiles we see in figure 4 are indicative of the type of wave like behaviour and orientation we observe in the unsteady flow.

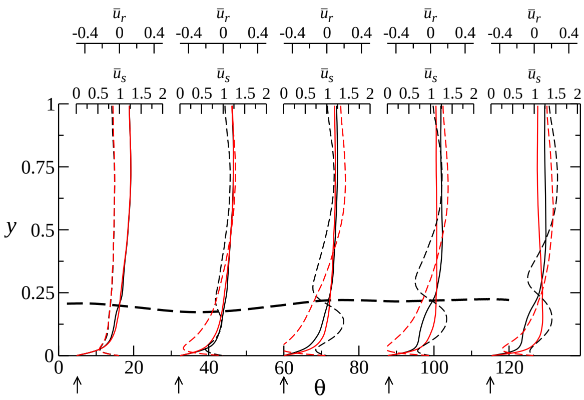

Figure 3: Mean radial velocity $\overline{u}_r$ (thin dashed line) and stream-wise velocity $\overline{u}_\theta$ (thin solid line) at $r = 4.5$ at $\theta = 5, 32, 60, 88, 115$ degrees for isothermal simulation (red line) and stratified flow (black line). Thick-dashed-line indicates the height where $\phi = 0.5$.

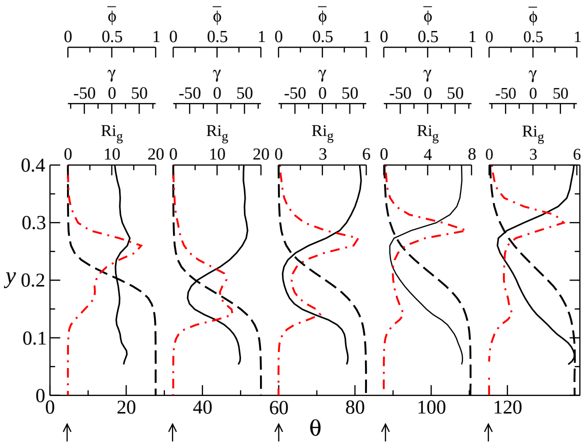

Figure 4: Mean gradient Richardson number Ri_g (red dashed-dotted line), γ (solid line) and $\overline{\phi}$ (dashed line) at $r = 4.5$ at $\theta = 5, 32, 60, 88, 115$ degrees for the stratified flow.

Conclusions

A comparison of isothermal and stratified open channel flow on a bend has been made using results from small scale direct numerical simulations. In the stratified flow we have observed a four layer flow structure, where the near bed lateral velocity is oriented towards the inner side wall. The flow in the upper region and through the pycnocline is consistent with previous field measurements where a three layer structure was observed. The identification of the unexpected near bed behaviour is potentially significant for sediment transport and erosion studies. This behaviour was observed throughout the bend.

In the stratified flow, the strong vertical variation in lateral velocity introduces a complex forcing on the mixing layer where the shear magnitude and orientation varies across the interface. Just below and just above the interface, the vertical shear is directed towards the outer side wall while in the center of the mixing layer it is oriented towards the inner wall. The mixing layer in this study is initially sharp with a stable Richardson number. After $\theta \approx 60^\circ$ the Richardson number decreases to $Ri_g \approx 1$ and an interesting mixing dynamic is observed. In the upper and lower regions of the interface the shear produces Kelvin-Helmholtz (K-H) like structures which have the same rotational sense. Between these regions, K-H structures are also observed but they rotate in the opposite direction. In this way the K-H structures are simultaneously produced at three vertical locations though the mixing layer and have rotational sense aligned with shear at these locations.

Acknowledgements

The authors gratefully acknowledge the support of the Australian Research Council (ARC). The first author was supported by ARC post-doctoral research fellowship DP110103417.

References

[1] Blanckaert, K., and H. J. D. Vriend, Secondary flow in sharp open-channel bends, *J. Fluid Mech.*, **498**, 2004, 353–380.

[2] Lacy, J. R., and S. G. Monismith, Secondary currents in a curved, stratified, estuarine channel, *J. Geophys. Res.*, **106**(C12), 31,2001,283–31,302.

[3] Lacy, J. R., M. T. Stacey, J. R. Burau, and S. G. Monismith, Interaction of lateral baroclinic forcing and turbulence in an estuary, *J. Geophys. Res.*, **108**(C3), 2003, 3089.

[4] Chant, R. J., and R. E. Wilson, Secondary circulation in a region of flow curvature: Relationship with tidal forcing and river discharge, *J. Geophys. Res.*, **107(C9)**, 2002, 3131.

[5] Nidzieko, N. J., J. L. Hench, and S. G. Monismith, Lateral circulation in well-mixed and stratified estuarine flows with curvature, *J. Phys. Oceanogr.*, **39**, 2009, 831–851.

[6] van Balen, W. , Blanckaert, K. and Uijttewaal, W. S. J., Analysis of the role of turbulence in curved open-channel flow at different water depths by means of experiments, LES and RANS, *J. Turbulence*, **11**, 12, 2010, 1–34.

[7] Constantinescu, G., Koken, M. and Zeng, J. The structure of turbulent flow in an open channel bend of strong curvature with deformed bed: Insight provided by detached eddy simulation, *Water Resour. Res.*, **47**, 2011, W05515.

[8] Kirkpatrick, M. P., and S. W. Armfield, Experimental and large eddy simulation results for the purging of a salt water filled cavity by an overflow of fresh water, *Int. J. Heat Mass Transfer*, **48**, 2005, 341–359.

[9] Gillam, N. L., Experimental and numerical investigation of density stratified mixing of saline fluid from a cavity within an open-channel bend using an overflow, Ph.D. thesis, The University of Sydney, 2010.

[10] Kirkpatrick, M. P., S. W. Armfield, and N. Williamson, Shear driven purging of negatively buoyant fluid from trapezoidal depressions and cavities, *Phys. Fluids*, **24**, 2012, 025106.

[11] Norris, S. E., C. J. Were, P. J. Richards, and G. D. Mallinson, A Voronoi based ale solver for the calculation of incompressible flow on deforming unstructured meshes, *Int. J. Numer. Meth. Fl.*, *65*, 2011, 1160–1179.

[12] Ferziger, J. H., and M. Perić, *Computational Methods for Fluid Dynamics*, Springer, 2002.